Petrogenetic processes at the tipping point of plate tectonics: Hf-O isotope ternary modelling of Earth's last TTG to sanukitoid transition

Hugo Moreira, Craig Storey, Mike Fowler, Luís Seixas, Joseph Dunlop

Petrogenetic processes at the tipping point of plate tectonics: Hf-O isotope ternary modelling of Earth's last TTG to sanukitoid transition

Hugo Moreira[a,b], Craig Storey[a], Mike Fowler[a], Luís Seixas[c] and Joseph Dunlop[a]

[a] School of the Environment, Geography and Geosciences, University of Portsmouth, Burnaby Building, Burnaby road, Portsmouth, PO1 3QL, UK;
[b] CNRS-UMR5243, Géosciences Montpellier, Université de Montpellier, 34095 Montpellier Cedex 05, France;
[c] Departamento de Engenharia de Minas - DEMIN, Universidade Federal de Ouro Preto - Campus Morro do Cruzeiro, Ouro Preto - MG, 35400-000, Brazil.

Highlights

Zircon Hf-O evidence supports recycled oceanic crust and continental crust growth during the magmatic lull;

Deep mantle penetration of subduction material marks a sporadic episode of sanukitoid magmatism;

Youngest TTG-sanukitoid transition is the last vestige of an ante-plate tectonics regime;

Global TTG-sanukitoid magmatic transition is a protracted, diachronous process and spans at least 800 Myr.

Abstract

Modern style plate tectonics is characterized by one-sided subduction and continental margin basalt-andesite-dacite-rhyolite (BADR) magmatism, whereas continental magmatic rocks in the Archaean record had tonalite-trondjhemite-granodiorite (TTG) composition. Their main difference is the absence (in the modern style) and the presence (in the ancient style) of abundant juvenile, basalt-derived felsic magmatism. The diversity of modern continental magmas depends partly on metasomatic processes in the mantle wedge providing sediment input (melt/fluid). Contrasting scenarios in the rock record therefore are the presence or absence of (1) basalt-derived melt (TTG) and (2) sedimentary input to the magmas. A late, "Archaean-style" tectonic regime is recorded in the Palaeoproterozoic Mineiro Belt (Brazil) using whole-rock geochemistry of its plutons coupled to zircon Hf and O isotopes from these rocks and from detrital grains from the local (meta)sediments. Increasing $\delta^{18}O$ with decreasing $\varepsilon Hf_{(t)}$ values in zircon indicate oceanic crust recycling and input of sediments to the mantle wedge during the Palaeoproterozoic. Since some form of early subduction including the formation of a mantle wedge has occurred since the Mesoarchaean, it seems that the onset of subduction and the final establishment of modern plate tectonics at the global scale are temporally distinct. The latter did not occur until the Palaeoproterozoic. Prior to this time ("ante-plate tectonics"), punctuated subcretion/subduction marks a gestational stage that took c. 800 Myr to transition diachronously to a truly global mechanism. The TTG-sanukitoid transition, which signals the opening of a mantle wedge, occurred in the Mineiro Belt during the early Proterozoic "magmatic lull" and thus represents the last gasp of the ante-plate tectonics regime.

Keywords: Subduction, Plate tectonics, TTG-sanukitoid transition, Hf-O zircon modelling

Corresponding author e-mail address: hugo.moreira@port.ac.uk

The authors have no competing interests to declare.

1 – Introduction

The composition of the early continental crust and the evolution of plate tectonics are subjects of current debate, with ideas varying from a stagnant mafic lid to a felsic and dynamic proto-crust (e.g. Bédard, 2018; Nebel et al., 2018; Cawood et al., 2018). However, the onset of mobile lid plate tectonics is widely inferred to have started at c. 3.0 Ga when early vertical tectonics progressed to a horizontal style (Beall et al., 2018 and references therein), although mobile lid behaviour in the evolution of Eoarchean terranes has been inferred in Greenland and Canada (e.g. Cawood et al., 2018; Nebel et al., 2018). By 3.0 Ga, several other lines of evidence suggest mobility of tectonic plates, marked by shallow subduction and increased reworking of previously-existing crust (e.g. Dhuime, et al., 2018; Cawood et al., 2018). During this period, magmatism was dominated by tonalite-trondjhemite-granodiorite suite rocks (TTGs), formed by partial melting of alkali-rich basalt sources (e.g. Moyen and Martin, 2012 and references therein; Moyen and Laurent, 2018) and/or melting of oceanic plateau basalts (Hastie et al., 2016). Sanukitoid magmas are petrogenetically more complicated successors to TTGs, being derived from mixed crustal and mantle reservoirs as indicated by high LILEs often with 'enriched' radiogenic isotopes and high $\delta^{18}O$, combined with high Mg# and transition metals (e.g. Shirey and Hanson, 1984; Martin et al., 2009). These characteristics have been explained by steepening of the subducted oceanic slab and consequent opening of a mantle wedge, which could then interact with slab-derived (i.e. crustal) fluids and melts (Moyen and Martin, 2012), including TTG magmas and/or subducted sediments. Therefore, the transition from TTG to sanukitoid magmas is often

inferred to mark the onset of subduction-driven plate tectonics caused by Earth's cooling, which then evolves to modern-style subduction-related magmatism (basalt-andesite-dacite-rhyolite - BADR, Fig. 1). Alternatively, this transition could have been caused by subcretion of plates or pseudo-subduction (Bédard, 2018), not characterising a regime of modern-style plate tectonics, but still providing evidence for plate mobility (Fig. 1).

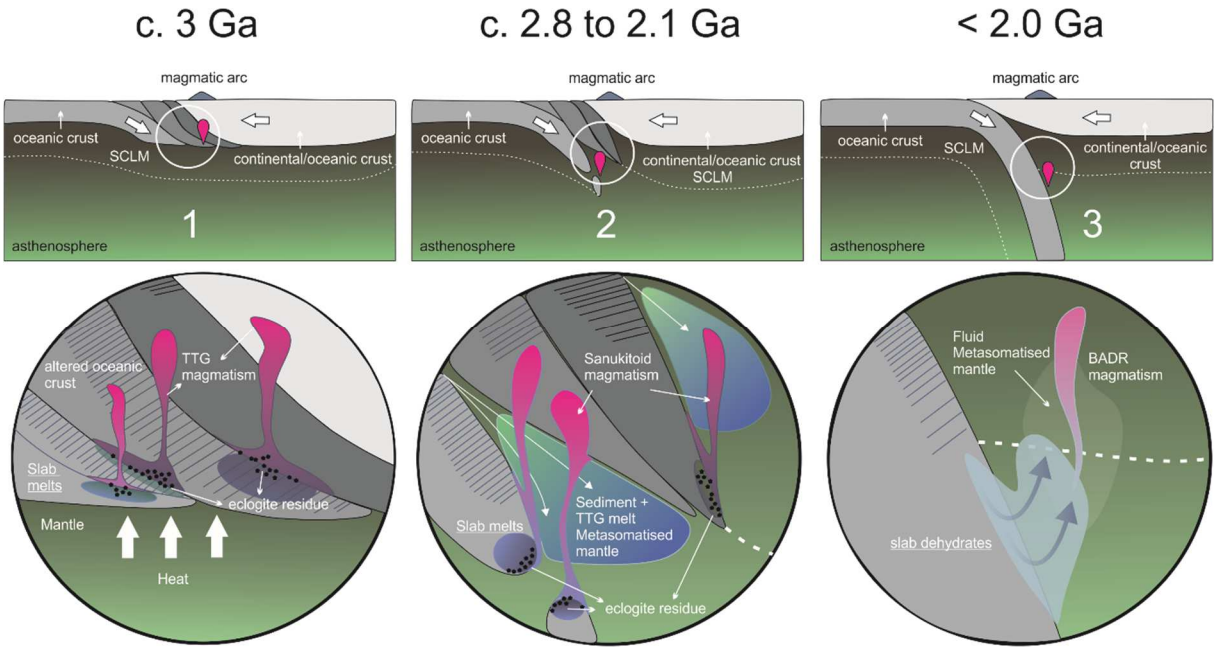

Figure 1: Diagrams with three tectonics scenarios for the Earth. Left: simplified geodynamics of an Archaean convergent setting characterized by stacking of oceanic slab and the lack of generation of mantle wedge and deep subduction. The subduction is mostly flat and the plate melts before it gets deep; produces TTG-like magmas and eclogite as residue. Centre: Sanukitoid magmas are formed in a 'thrust belt subcretion' scenario. The TTG magmas interact with a mantle wedge metasomatised by sediments and/or previous interaction with older TTG melts. Right: simplified geodynamics of a Phanerozoic convergent setting with deep subduction and dehydration of the plate. In all three scenarios, there are lateral and vertical movement of the edge of plates (i.e. plate tectonics is active), but because of different geothermal conditions and rheology of the different scenarios, the panel on the left and central case are not considered subduction in this study, but subcretion.

There is a trend in the current literature to establish a modern plate tectonic regime at the boundary between the Archaean and Palaeoproterozoic, meaning 2.5 Ga (e.g. Cawood et al., 2018 and references therein), but two points have yet to be fully understood: firstly, the TTG-sanukitoid transition was diachronous over nearly 1 Ga

because the last documented transition occurred from 2.35 to 2.1 Ga (Moreira et al., 2018); therefore the same tectonic scenarios must have coexisted on Earth from c. 3 to 2 Ga, even if in different proportions. The second point is that if TTGs and sanukitoids were not formed by what is considered modern subduction tectonics (e.g. Stern, 2018), it should be argued that the latter did not operate before 2.1 Ga, as opposed to what is converging as an agreement in the literature (e.g. Nebel et al., 2018; Cawood et al., 2018).

In this study, we contribute to the current debates surrounding the secular evolution of granitoids and whether horizontal tectonics require modern-style subduction. For this, we present oxygen, U-Pb and Lu-Hf isotope data in zircons from igneous and sedimentary rocks of the early Proterozoic Mineiro Belt, Brazil. The three isotope systems combined have long proved to be a powerful tool in understanding tectonic settings, magma generation, recycling and crustal growth (e.g. Hawkesworth and Kemp 2006; Hopkinson et al., 2017). The Mineiro Belt rocks contain the youngest TTG-sanukitoid geochemical transition yet reported (c. 2.1 Ga), and thus represent the final vestige of the earlier regime, after which plate tectonics was truly global. They also occupy the proposed (but narrowing) global magmatic lull and therefore contribute to knowledge of a period when little 'juvenile' magmatism is known (Spencer et al., 2018). The data are used to place constraints on TTG and sanukitoid petrogenesis at 2.1 Ga and are further compared to well-established Archaean TTG-sanukitoid provinces. Ultimately, the data have implications for both the proposed subcretion regime in plate tectonics and the contribution of early mantle-derived sources in younger juvenile terranes. Overall, we advocate non-modern subduction (ante-plate tectonics) on Earth prior to 2.1 Ga, when the first low dT/dP rocks also appeared and modern calc-alkaline magmas began to dominate the geological record (Brown and Johnson, 2018).

2 – Geological context

The São Francisco Craton (SFC) comprises a mosaic of various Archaean blocks composed of TTGs and greenstone belts sutured in the Palaeoproterozoic at around 2.1 Ga and shielded from magmatism and significant deformation/metamorphism from a later Neoproterozoic orogeny (e.g. Heilbron et al., 2017 and references therein) (Fig. 2a). The Palaeoproterozoic occurrences are broadly discriminated either as Archaean reworked palaeocrust or juvenile arcs/plateaus. The current margins of the craton mark its last deformation during the Neoproterozoic (Heilbron et al., 2017) (Fig. 2b). The area of interest in this study encompasses the southern portion of the SFC, where the Archaean basement is bounded to the south by a geologically distinct terrane, known as the Mineiro Belt (Fig. 2c). The terminology palaeocraton, which follows, denotes any of the Archaean portions of the craton amalgamated in the Palaeoproterozoic.

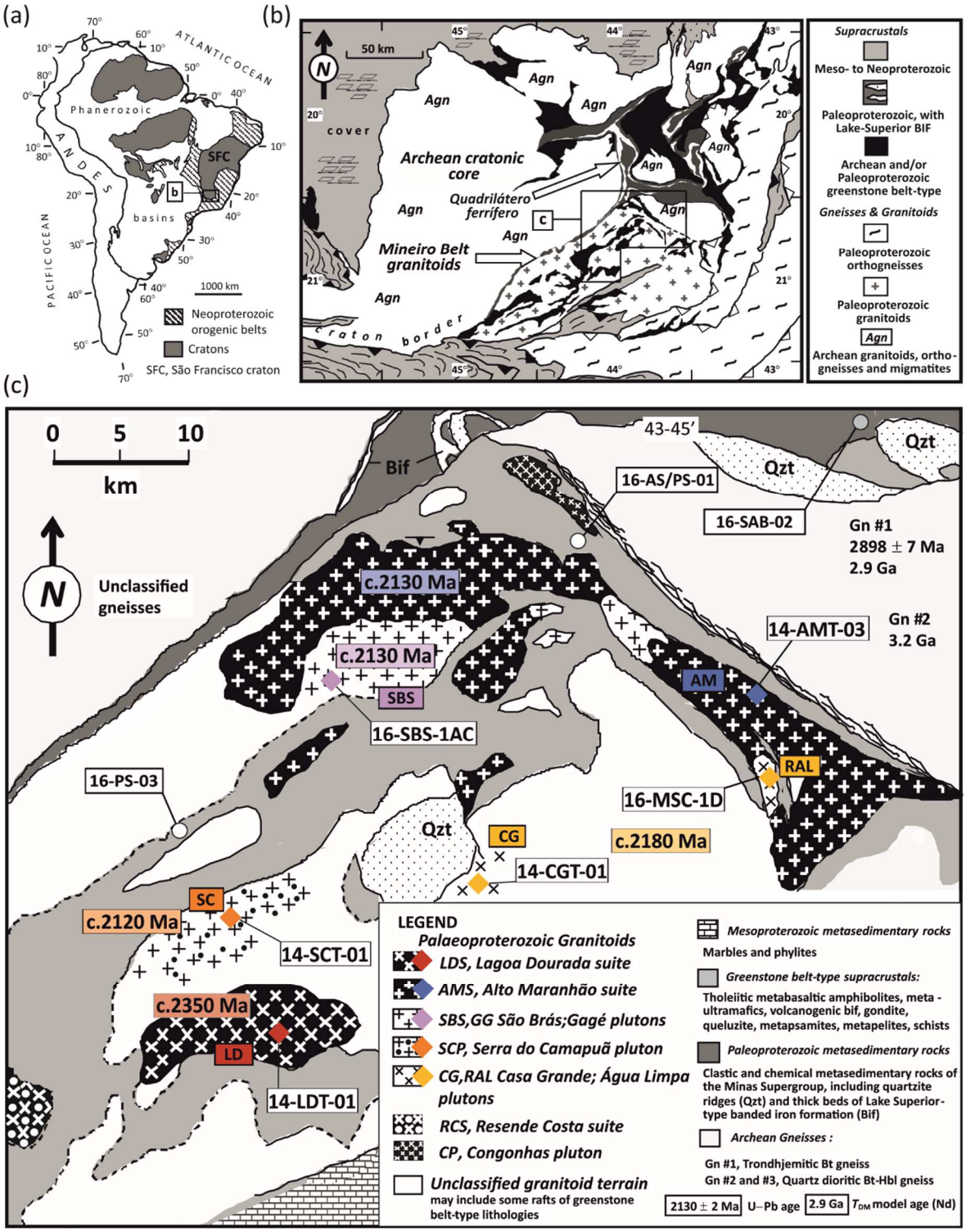

Figure 2: Location of Paleoproterozoic granitoids of the Mineiro Belt in the São Francisco craton (SFC). Adapted from Seixas et al. (2012) and references therein. (a) The SFC in relation to the major tectonic units of South America. (b) Location of the Mineiro Belt within the southern SFC. (c) Sampling localities investigated in this study.

The Mineiro Belt represents a juvenile Palaeoproterozoic crustal segment (Teixeira et al., 2015; Moreira et al., 2018 and references therein). Its west sector, which comprises more than 6000 km^2 of crust almost unaffected by a younger Neoproterozoic

orogeny, is in stark contrast to the rest of the Palaeoproterozoic crust in the region, shown in Figure 2b as orthogneisses. These chronologically-correlated segments to the east - the Juiz de Fora and Mantiqueira complexes - were intensely overprinted by metamorphism up to granulite facies with voluminous partial melting in the Neoproterozoic (e.g. Heilbron et al., 2017). Therefore, distinguishing the Palaeoproterozoic features in those terranes is inevitably hampered by the Neoproterozoic orogenic overprint, which makes the relatively unaffected Mineiro Belt a regional reference for geological investigation and extrapolation to the more deformed terranes. Moreover, the Mineiro Belt contains both TTG and sanukitoid suites, respectively known as the Lagoa Dourada suite (Seixas et al., 2012) and the Alto Maranhão suite (Seixas et al., 2013). Together, they are comparable to and can be categorised as most other Archaean TTG to sanukitoid transitions in many cratons worldwide (e.g. Halla et al., 2017; Laurent, et al., 2014). Their characteristic elemental geochemistry is summarised in Figure 3 (a-d). All studied granitoids have intermediate SiO_2 and show relative HREE depletion with absent to positive Eu anomalies (enclaves sometimes show 'false negative' Eu anomalies generated by abundant middle-REE-rich minerals - Seixas et al., 2013). The Lagoa Dourada Suite shows depletion of LILE, and plots in the TTG field from Laurent et al. (2014) (red diamonds – Fig. 3). The sanukitoids (SiO_2 = 60 to 66 wt.%) and hosted mafic co-magmatic enclaves (SiO_2 = 48 to 55 wt.%) have the highest content of Ba+Sr, Cr and Mg# among the magmas studied (dark and light blue diamonds, respectively – Fig. 3). Previous work using zircon Hf isotope and whole-rock Nd isotope model ages demonstrates that these two suites have sources extracted from the mantle between 2.50 and 2.45 Ga ago which evolved isotopically towards 2.0 Ga (Moreira et al., 2018). These authors conclude that the metasomatism of the mantle wedge generating the sanukitoid suite was caused by TTG melts such as the

Lagoa Dourada suite (Seixas et al., 2013), in the same way as in other cratons worldwide (Moyen and Martin, 2012). In addition to the sanukitoids, a related high Ba-Sr suite (Fig. 3) is thought to have formed by later fractional crystallisation and/or melting of the region above the mantle wedge (Moreira et al., 2018), on the basis of slightly higher SiO_2 content (67 wt.%) and depletion in compatible elements (pink diamonds - Fig. 3). A contemporaneous pluton has lower Ba+Sr content, Mg# and Cr; and plots in the hybrid field of Laurent et al., (2014) (orange diamonds - Fig 4). The Mineiro Belt also contains collision-related granitoids (Teixeira et al., 2015), metavolcanics/sedimentary sequences deposited at 2.088 ± 0.012 Ga (Ávila et al., 2014) and less abundant granitoids derived from Archaean mafic sources, crystallized between 2.18 and 2.2 Ga (Moreira et al., 2018) (yellow diamonds – Fig. 3). A volcanic to sub-volcanic unit, the Serrinha-Tiradentes suite (Ávila et al., 2014), marks an important period of juvenile accretion at 2.23 to 2.22 Ga along with a syn-sedimentation volcanoclastic sequence deposited on top of the São Francisco palaeocraton hinterland, known as the Sabará Group. The Sabará Group contains detrital zircons aged between 2.1 and 2.3 Ga with juvenile signatures ($\varepsilon Hf_{(t)} > 0$) and the youngest grains indicate a maximum depositional age of 2.125 ± 0.004 Ga (Martínez Dopico et al., 2017 and references therein). Importantly, not only the late TTG-sanukitoid transition, but the detrital zircon grains found by Martínez Dopico et al. (2017) are attributable to a period otherwise known as a 'tectono-magmatic lull' due to the relative scarcity of global magmatism in the geological record (Spencer et al., 2018). Thus, understanding the tectono-magmatic evolution of the Mineiro Belt has important global implications and also brings new insights into continental crust evolution and the development of plate tectonics.

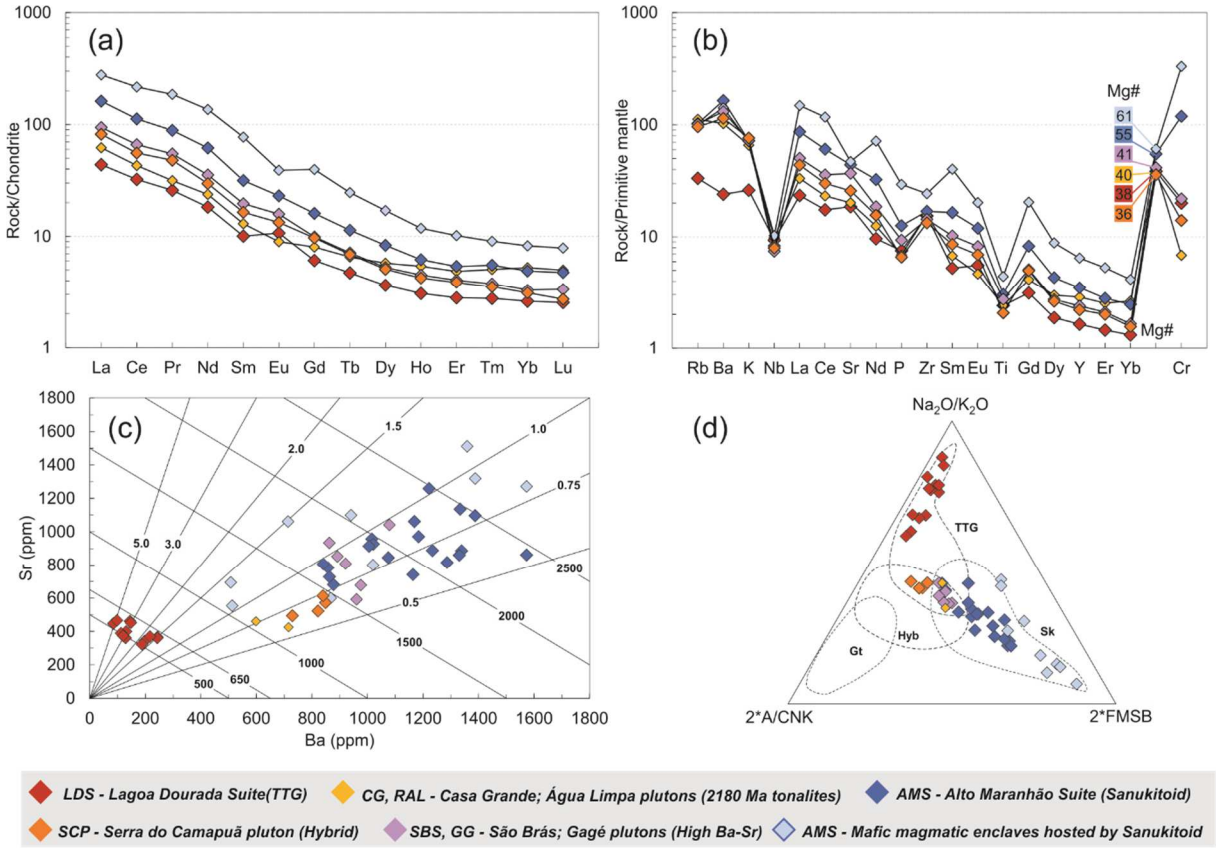

Figure 3: Geochemical parameters selected from the investigated samples. (a) REE normalized to C1 chondrite (Taylor and McLennan, 1985). (b) Pattern of trace elements normalized to the primitive mantle (Sun and McDonough, 1989). Note in this diagram the introduction of the non-normalized values of the parameters 100 * Mg # [= 100 * mol MgO / MgO + 0.9 * Fe_2O_{3t}] and Cr (ppm); (c) Ba versus Sr diagram, with the isovalue lines of the Sr / Ba (0.5 to 5.0) and Sr + Ba (500 to 2500 ppm). (d) Ternary diagram of classification of Neoarchaean granitoids as suggested by Laurent et al. (2014). Triangle vertices are: 2 * A / CNK (molar Al_2O_3 / (CaO + K_2O + Na_2O); Na_2O / K_2O wt.% ratio; and 2 * (FeO_t + MgO) vs (Sr + Ba) wt.% (FMSB). The TTG, Sk, Hyb and Gt fields designate TTG, sanukitoids, hybrid granitoids and granitic (*s.s.*) suites respectively. Plots in (a) and (b) are arithmetic mean values, LD suite (n = 12, data from Seixas et al., 2012); AM suite, tonalite host (n = 15, data from Seixas et al., 2013); AM suite, MME (dioritic mafic magmatic enclaves, n = 9, data from Seixas et al., 2013); RAL suite (n = 1, from Moreira et al., 2018); High Ba-Sr suite, n = 3, from Moreira et al., 2018); Hybrid suite, n = 3, from Moreira et al, 2018). In (c) and (d) all data from these suites of the articles by Seixas et al., 2012;2013 and Moreira et al., 2018 are included.

3 – Samples and Methods

The granitoids in this study include TTG, sanukitoid, high Ba-Sr and 'hybrid' granitoids (*sensu* Laurent et al., 2014) from Moreira et al. (2018), to which the reader is directed for a full description and detailed interpretation. The labelling scheme herein is also the same, for clarity. In addition, four metasedimentary samples, three from within the Mineiro Belt area and one from the palaeocraton domain have been analysed (Fig. 2c). These samples contain detrital zircons and thus potentially represent a more comprehensive sampling of eroded equivalents to the individually-sampled granitoids

and their host lithologies. The samples from the Mineiro Belt are metagreywackes located at the centre of the belt (16-PS-03) and at its margins with the palaeocraton (16-AS-01 and 16-PS-01). The fourth sample belongs to the Sabará Group and is a metadiamictite with clasts of carbonates, granitoids, quartzites, phyllites and banded iron formation, ranging in size from 1 to 15 cm. In total, 387 oxygen isotope analyses of unknown zircon grains were performed using the NERC Ion Micro-Probe Facility (Cameca 1270) at the University of Edinburgh, Scotland prior to U-Pb and Lu-Hf analyses at the University of Portsmouth, UK. At Portsmouth, a 193 nm RESOlution ArF Excimer laser was coupled to an Analytick Jena PlasmaQuant Elite ICP-MS for the U-Pb analyses; and subsequently to a Nu Plasma I MC-ICP-MS for the Hf analyses.

Zircon grains with U-Pb analyses more than 5% discordant were not considered for interpretation due to well-known disturbances caused in oxygen and Lu-Hf isotope systems. U-Pb discordance potentially implies isotopic alteration in oxygen analyses and also leads to uncertainty in crystallisation age, consequently affecting the derivation of accurate initial Hf isotopic ratios. Usually, these effects modify both indices ($\delta^{18}O$ and $\varepsilon Hf_{(t)}$) to lower values (e.g. Valley, 2003; Payne et al., 2016). However, all analyses are presented in supplementary material. Some of the zircon grains with enough space in the compositional domain were ablated twice for U-Pb, after having been analysed for oxygen. Analyses yielded the same ages within uncertainties when compared to analyses previously performed in different grains from the same samples (*cf.* Moreira et al., 2018). Lu-Hf analyses were then carried out on top of the previous oxygen and U-Pb pits. Complete methodology, description of the sedimentary samples and analytical conditions are provided in the supplementary material.

4 – Results and preliminary interpretation

Table 1 summarizes the results obtained in this study. A detailed description is provided in the following paragraphs, summarized graphically in Figure 4.

Table 1: Compilation of data obtained in this study for the igneous zircon grains. Abbreviations PS and AS stand for Palaeoproterozoic and Archaean Source, respectively. Symbols (c) and (r) represent analyses performed in the core or rim. Sedimentary rocks were omitted.

Sample	Suite	Age (Ga)	$\varepsilon Hf_{(t)}$ (avg)	$\varepsilon Nd_{(t)}$[a]	$^{Hf}T_{DM}$[a] (Ga)	$^{Nd}T_{DM}$[b] (Ga)	Oxygen $\delta^{18}O$ ‰ (avg)
14-LDT-01	TTG (PS)	2.350	+3.3 to +6.6 (+4.7)	+1.0 to +2.1	2.41 to 2.61	2.4 to 2.5	+4.2 to +5.0 (+**4.6**)
16-MSC-1D	TTG(AS)	2.170 – 2.180	-0.9 to -4.7 (-2.7)	-2.9	2.67 to 2.93	2.6	+5.1 to +5.9 (+**5.5**)
14-CGT-01	TTG(AS)	2.170 – 2.180	+0.7 to -5.0 (-2.4)	-	2.66 to 2.91	-	+4.8 to +5.7 (+**5.3**)
14-AMT-03	Sanukitoid	2.130	-0.4 to +1.4 (+0.5)	-1.0 to +0.9	2.45 to 2.69	2.3 to 2.4	+4.7 to +6.7 (+**6.3**)
16-SBS-1A	High Ba-Sr	2.130	+2.0 to -1.3 (+0.2)	+0.3	2.48 to 2.72	2.3 to 2.4	+5.9 to +7.5 (+**6.8**)
14-SCT-01	Hybrid	2.120 – 2.130	+0.8 to -2.4 (-0.9)	-1.2 to -0.8	2.52 to 2.77	2.5	+3.9 to +6.2 (+**5.6**)

[a] Range of values based on average of model ages after calculations using different constants (see supplementary file for details).
[b] Data compiled from Seixas et al. (2012; 2013) and Moreira et al. (2018).

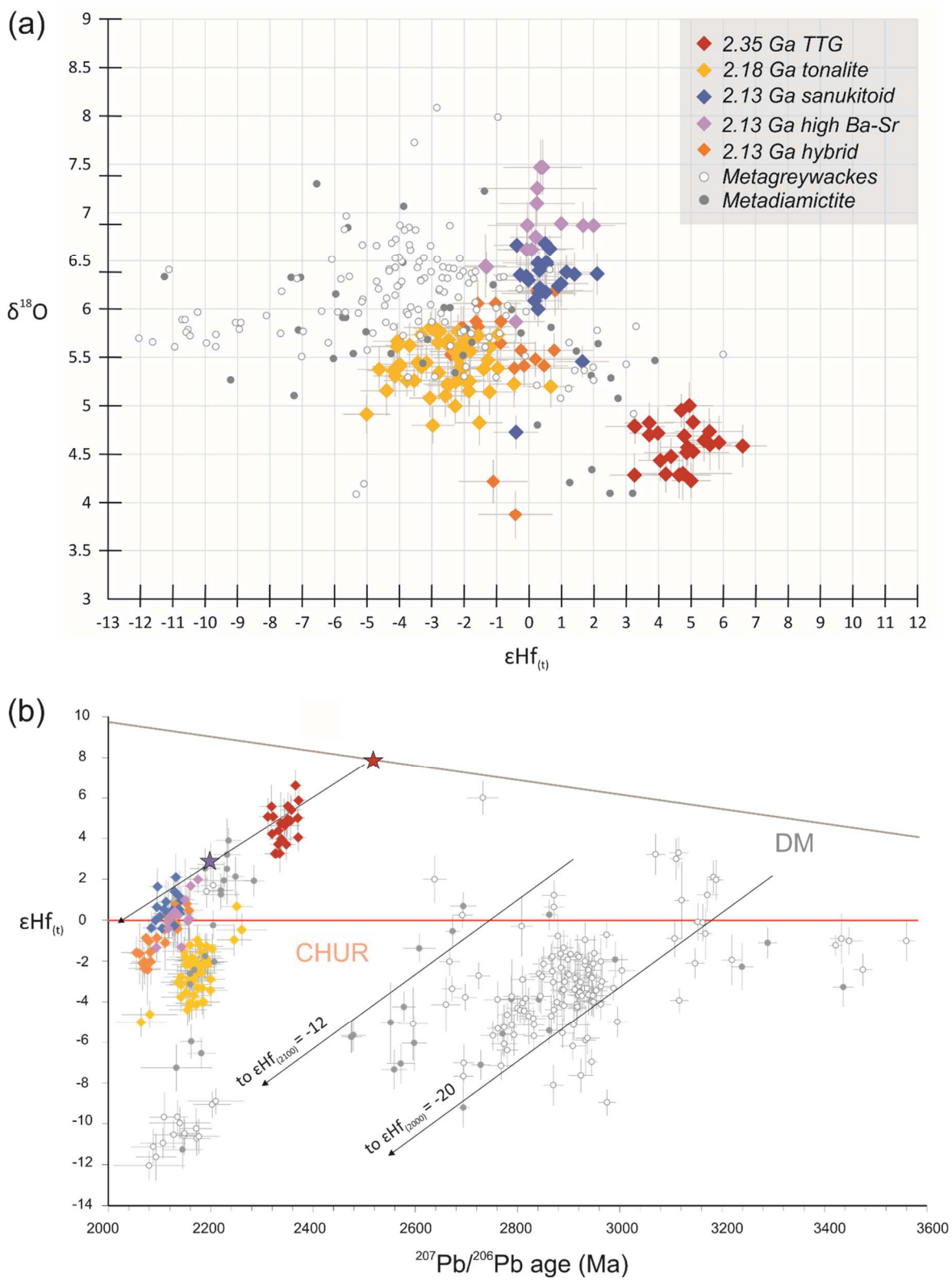

Figure 4: Oxygen and hafnium isotopic composition of zircons from plutonic and sedimentary rocks of the Mineiro Belt, Brazil represented in $\delta^{18}O$ (relative to VSMOW) and εHf notation for the diagram in panel (a) and $^{207}Pb/^{206}Pb$ age versus εHf in panel (b). Igneous zircons are colour-coded following figure 2. Filled grey circles are detrital zircon grains from the foreland basin meta-sediments and the open circles are detrital grains from the metagreywackes within the belt. Error bars for both diagrams are 2σ confidence level. Panel (b) shows proposed evolution lines in εHf-age space. Red star represents extraction from the depleted mantle (DM) and purple star represents potential mantle composition at c. 2.2 Ga. See details for DM and CHUR parameters in the supplementary material.

253 *4.1 – Igneous rocks*

254 4.1.1 Tonalite – trondhjemite-granodiorite suite (TTG)

255 U-Pb analyses carried out on zircon grains from the garnet-bearing high-Al TTG –
256 Lagoa Dourada suite yielded concordant ages (all > 96% concordance) with weighted
257 mean average of 2.344 ± 0.0057 Ga (MSWD = 1.1). The concordant grains have a
258 weighted average age of 2.342 ± 0.01 Ga (MSWD = 1.0). $^{176}Hf/^{177}Hf$ zircon analyses
259 record initial mean compositions that are considerably above CHUR; $\varepsilon Hf_{(t)}$ values cluster
260 between +3.26 and +6.6 and average +4.65. Oxygen isotope analyses yield $\delta^{18}O$ values
261 between +4.2 and +5.0 ‰. Together, the narrow range of both values are consistent
262 with a young mafic oceanic crust source that had been altered to some extent by surface
263 processes (e.g. Hiess et al., 2009), thus modifying the O-isotope signature.

264 Tonalites of 2.18 and 2.2 Ga age contain metabasaltic xenoliths with ~3.3 Ga
265 Archaean model ages (Seixas et al., 2013). Country rock assimilation has been suggested
266 as an explanation for $\varepsilon Nd_{(t)}$ values as low as -2.9 (Moreira et al., 2018). The εHf values
267 down to -5.0 $\varepsilon Hf_{(t)}$ (average -2.6) are in agreement with the -2.9 $\varepsilon Nd_{(t)}$ whole-rock
268 signature, but zircon $\delta^{18}O$ values reflect mantle derivation. Indeed, 57 out of 61 grains
269 have $\delta^{18}O$ values between +5.1 ± 0.21 ‰ and +5.9 ± 0.15 ‰ (average +5.5 ‰). The
270 other four grains have slightly lower $\delta^{18}O$, down to +4.8 ± 0.2 ‰. Thus, it is more
271 plausible that tonalites were derived from Archaean mafic crust that resided in the
272 lower crust of the Mineiro Belt for up to 800 Myr, but with insignificant supracrustal
273 contamination which would have modified $\delta^{18}O$ towards higher values. This long
274 residence time is required to explain the Hf and Nd isotope evolution, from extraction of
275 source at c. 3.0 Ga to re-melting at 2.18 Ga.

276 4.1.2 Sanukitoids and associated rocks

277 The youngest igneous rocks of this study are c. 2.13 Ga old and are divided in to
278 three distinct groups: sanukitoids (Alto Maranhão Suite) marked by LILE enrichment
279 (specially Ba and Sr) with high Mg, Ni and Cr; high Ba-Sr granitoids with significantly
280 lower compatible elements; and hybrid granitoids rather less enriched in Ba and Sr (Fig.
281 3) and endowed with some crustal inheritance (identified by Archaean inherited zircons
282 and older model ages).

283 For the sanukitoids, eleven concordant zircons with $^{207}Pb/^{206}Pb$ age ranging from
284 2.102 ± 0.036 Ga and 2.140 ± 0.043 Ga yielded $\delta^{18}O$ values between +6.18 and +6.68 ‰
285 (average +6.35 ± 0.22 ‰). Twenty-two other zircons with concordance varying from 95
286 to 103 % have $\delta^{18}O$ values between +4.7 and +6.7‰ (average +6.2 ‰). The $\varepsilon Hf_{(t)}$ values
287 of the concordant zircons are essentially chondritic to slightly super-chondritic (+0.3 to
288 +1.15); the slightly discordant grains average +0.47 with some values as low as -0.4, the
289 latter likely an artefact caused by discordance (e.g. Payne et al., 2016). The oxygen
290 isotope signatures range up to +6.7‰ and likely reflect a sedimentary contribution in
291 the magma source, possibly from subduction-related enrichment of the mantle (e.g.
292 Fowler et al., 2008; Heilimo et al 2013). Incorporation of supracrustal material within
293 the crust is not a viable interpretation of the high $\delta^{18}O$ values because 1) the sanukitoid
294 does not contain xenoliths of any nature, only abundant co-magmatic andesitic-basaltic
295 enclaves; 2) the whole rock $\varepsilon Nd_{(t)}$ and zircon $\varepsilon Hf_{(t)}$ values are essentially chondritic with
296 no evidence of interaction with older crust; and 3) older crust in the region has much
297 lower Ba-Sr content. Therefore, enrichment must have happened in the magma source.

298 The high Ba-Sr granitoids yielded $^{207}Pb/^{206}Pb$ ages ranging from 2.094 ± 0.038 Ga
299 and 2.175 ± 0.040 Ga (average of 2.136 ± 0.034 Ga) and $\delta^{18}O$ values between +5.9 and
300 +7.5 ‰ (average +6.8 ‰). The $\varepsilon Hf_{(t)}$ values vary from -1.3 to +2.0 and therefore closely

overlap those of the sanukitoids. Since they have only marginally higher $\delta^{18}O$ a genetic link is possible, perhaps via fractional crystallisation of the same or similar magma. The third group (hybrid granitoids) yielded zircons ages between 2.061 ± 0.046 Ga and 2.158 ± 0.037 Ga and $\delta^{18}O$ values between +3.9 ± 0.25 and +6.18 ± 0.26 ‰ (average +5.6 ‰) with no clear relationship between age and oxygen isotope signature. The $\varepsilon Hf_{(t)}$ values are distinctly more negative than the first two groups, ranging from +0.8 to -2.4 with the least radiogenic signatures (i.e. lower $\varepsilon Hf_{(t)}$) in the youngest grains.

4.2 – Sedimentary rocks

Detrital zircon grains from metagreywacke samples have a general bimodal age distribution in probability histograms with ages varying from 2.080 to 3.560 Ga. The main peak is around 2.9 Ga and the youngest subordinate peak is around 2.1 Ga (Fig. 5a). The meta-diamictite has a similar range of detrital zircon ages, but the distribution is distinct: the highest peak is around 2.1 Ga and there are several smaller peaks as old as 3.3 Ga. The three metagreywacke samples were deposited in an extensional/passive margin setting identified by the higher proportion of Archaean inheritance compared to the maximum depositional age of 2.090 Ga (see supplementary material for explanation on the maximum depositional age) (Cawood et al., 2012) (Fig. 5). Thus, the lack of significant inheritance in the plutonic rocks of the belt contrasts significantly with the detrital zircon spectra. This can be explained either by complete melting of xenocrystic zircons in high temperature magmas, little contamination or zircon-absent local crust during emplacement. The latter would imply that the Archaean detrital zircon grains come from the SFC to the north and the crust traversed and intruded by the granitoids was predominantly mafic.

The sample collected from the Sabará Group in the palaeocraton domain shows a typical foreland-type detrital zircon spectrum (Fig. 5). Zircon grains with ages close to the 2.2 Ga volcanic arcs in the region (Ávila et al., 2014) are mostly juvenile according to the Hf and oxygen isotopes (averages $\varepsilon Hf_{(t)}$ and $\delta^{18}O$ for c. 2.2 Ga grains are +2.3 and +4.9 ‰, respectively). The grains with ages close to the maximum depositional age (c. 2.125 Ga) have $\delta^{18}O$ values averaging 5.9 ‰ and $\varepsilon Hf_{(t)}$ as low as -7. Archaean secondary peaks correlate to the palaeocraton sources (e.g. Teixeira et al., 2015). Strikingly, the oxygen and hafnium isotopic compositions of the detrital zircons do not overlap with most of the igneous zircons. This suggests that these igneous rocks were absent from the sedimentary provenance. Moreover, $\delta^{18}O$ values up to 8‰ together with εHf values down to -12 indicate recycling of the crust during the Archean. Archaean growth episodes are more prominent at c. 3.0 Ga, where detrital zircon grains have super-chondritic εHf and $\delta^{18}O$ values compatible with mantle melts (Fig. 4).

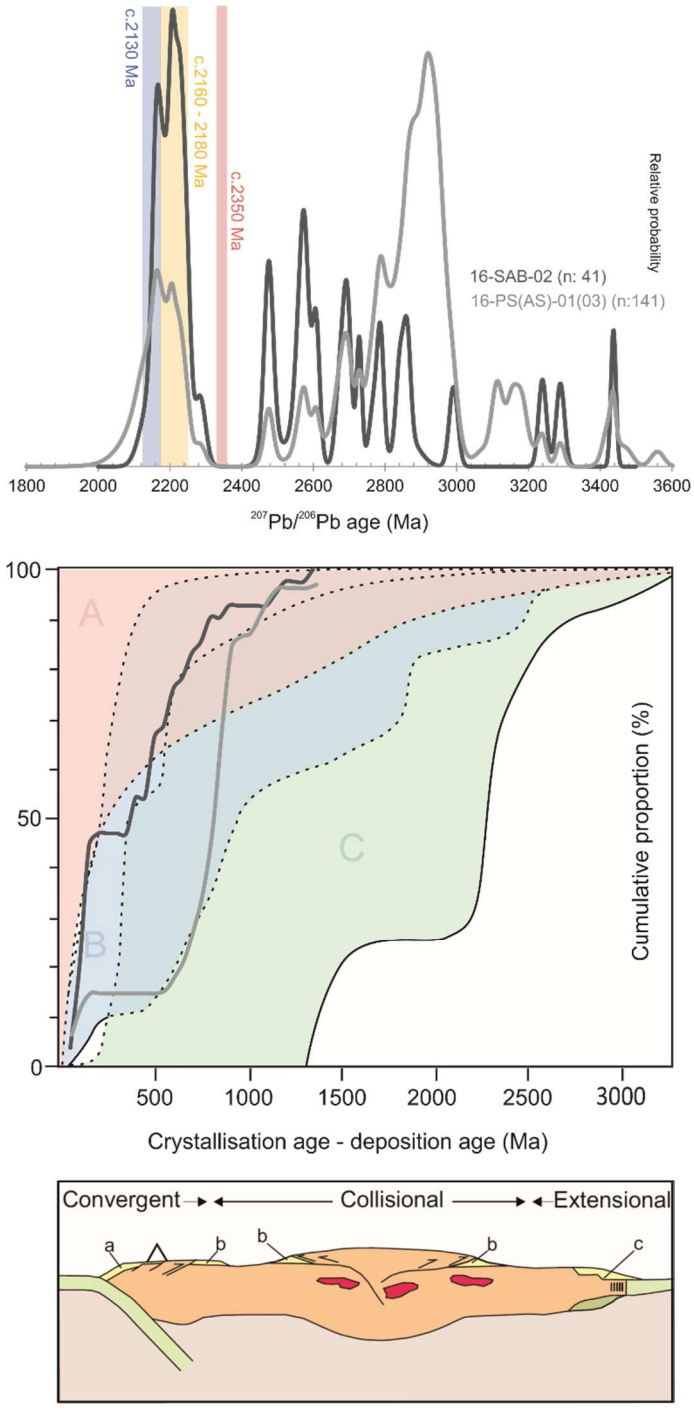

338

339 **Figure 5:** Probability density distributions of the detrital zircon ages show three main characteristics: 1)
340 Several older age peaks have no correspondence with magmatic events in the Mineiro Belt; 2) Largest
341 contribution of ages are different in the two sedimentary units of this study; 3) Detrital zircon grains do
342 not record age peak within the c. 2.35 Ga TTG magmatic event interval. Diagram from Cawood et al.
343 (2012) shows cumulative proportion curves of the crystallisation age of the detrital zircon grains minus
344 the deposition age of the sedimentary unit on x-axis. The diagram indicates the tectonic settings in which
345 the sediments were deposited, for which A, B and C fields on the diagram relate to a,b and c on tectonic
346 cartoon. The metagreywackes plot towards the extensional/passive margin field (grey curve), whereas
347 the syn-orogenic metasedimentary rock plots on the convergent/collisional foreland basin field (black
348 curve). Metagreywackes from the belt have a higher contribution of Archaean grains compared to the
349 maximum depositional age at 2.09 Ga. The detrital zircon distribution for this sample contrasts drastically
350 to the zircon ages in the plutonic rocks, which suggests distant cratonic areas as the main sources for the
351 passive margin basin.

5 – Discussion

5.1 – TTGs and sanukitoid magma generation

Most TTGs are derived from mafic rocks, themselves derived from undepleted mantle and comprise the majority of intermediate Archaean igneous rocks (e.g. Moyen and Laurent, 2018). Nonetheless, superchondritic zircon grains derived from TTGs are reported in this study and in other occurrences worldwide, indicating a depleted mantle source (see also Fig. 4). Hydration and alteration of the mafic source seems to be a fundamental prerequisite, but they could be derived from mafic oceanic plateaus (Hastie et al., 2016), in a shallow subduction style (Moyen and Martin, 2012) or in a thickened mafic crust (e.g. Smithies, 2000). The melting conditions of the mafic sources range significantly, from below 10 to more than 25 kbar, which yields a large pressure-dependent mineralogical range of residues during and after TTG-melt extraction (Foley et al., 2003), and therefore results in significant trace element variation (Moyen and Martin, 2012). Conversely, Laurent et al. (2020) have recently proposed that this whole geochemical variation can be a result of crystal-fractionation of a single tonalitic source formed by basaltic melting or differentiation in the lower crust (at <40 km depth). A broadly-chondritic reservoir is a consistent source for the generation of most TTGs, because an undepleted mantle is likely to melt more easily than any subsequent depleted mantle reservoir (e.g. Moyen and Laurent, 2018). As such, depleted mantle continues to grow at the expense of more primitive mantle (Moyen and Laurent, 2018) and it has been suggested that exhaustion of the latter coincides with the proposed ca. 2.4 – 2.2 Ga magmatic lull (Spencer et al., 2018). Therefore, TTG and sanukitoid generation in the Mineiro Belt could represent the global 'last gasp' of this transitional magmatism.

As outlined above, the enrichment in LILE (especially Ba and Sr) alongside the characteristic high Mg#, Cr and Ni of sanukitoids require at least two end-members: an ultramafic component has somehow to be enriched in LILE by the second component (e.g. Smithies, 2000). Sanukitoids are commonly thought to derive from the interaction between a TTG-like melt (± sediments) and mantle peridotite (Martin et al., 2009; Moyen and Martin, 2012), but there are many variations upon that theme. A lack of or small positive Eu anomaly associated with Sr enrichment suggests the absence of plagioclase in the residue and hence a deeper source (Moyen and Martin, 2012).

Some of the tectonic mechanisms proposed that are consistent with these constraints include dehydration and melting of a subducted oceanic slab (e.g. Fowler et al., 2008), slab break-off (Halla et al., 2009), and/or two-stage metasomatisation with mantle upwelling and delamination of the subcontinental lithospheric mantle (Heilimo et al., 2010). Each could explain the origin of specific magmas, but the latter attempts also to explain the paradox of magmas with similar geochemical characteristics but different isotopic signatures. The model explains, for example, the reason why magmas with a sediment contribution may not have enriched εHf/εNd composition, and predicts an explanation for a major element distinction between low and high-Ti sanukitoids, based on modelling between degree of melting and enrichment of the source (Martin et al., 2009). Similarly, Laurent et al. (2014) regard aspects of crustal reworking as markers of sanukitoid generation through time, because increasingly negative εNd and εHf isotopic features can be a consequence of old sediment intake into the mantle wedge. Notwithstanding these details, given the geochemistry, broadly-chondritic εHf and generally high $\delta^{18}O$ values of the 2.13 Ga plutonic rocks from the Mineiro Belt, they probably interacted with a mantle wedge at some point in their history. This hypothesis

400 is tested and constrained with a novel three-component Hf-O isotope mixing model,
401 discussed below.

402 *5.2 – A zircon-based mixing model between mantle, TTG-melt and sediments*

403 Zircon grains that grew in equilibrium with mantle melts retain a $\delta^{18}O$ isotopic
404 signature at around 5.3 ± 0.6‰ (Valley, 2003). Those that crystallised from magmas
405 with variable incorporation of supracrustal material will have a proportionally higher
406 $\delta^{18}O$ (e.g. Hopkinson et al 2017), since oxygen isotopes fractionate strongly under low-
407 temperature surficial processes due to the large positive mineral-water fractionation
408 factors at low temperature (Zheng, 1993). Conversely, high-temperature hydrothermal
409 activity (T> 400°-500°C) may modify $^{18}O/^{16}O$ to lower $\delta^{18}O$ during alteration of oceanic
410 crust at deeper levels (>2.5 km) (Gregory and Taylor, 1981). This is because at high T,
411 mineral-water fractionation factors are low so that interaction with seawater ($\delta^{18}O$ = 0)
412 is able to produce rock values lower than those of the mantle (Zhao and Zheng, 2003).
413 Hafnium isotope model ages may be used to estimate protolith separation age from a
414 mantle reservoir, and the combination of both is a powerful tool in crustal evolution
415 research (e.g. Kemp et al., 2006; Dhuime et al., 2018 and references therein). For
416 example, reworking arrays sometimes generated by regional data (when they show
417 similar regression towards the mantle reservoir) may represent major crustal growth
418 events, within which oxygen isotopes can help constrain the juvenile contribution.
419 Although there is an increasing debate about model ages (Payne et al., 2016 and
420 references therein), the applicability of the approach alongside accurate U-Pb zircon
421 ages, to constrain evolved versus juvenile signature in εHf-time space, is not in doubt.

422 In this study, oxygen isotopes do not correlate clearly with most whole-rock
423 parameters. However, the samples with the highest Ba plus Sr content have the highest

424 $\delta^{18}O$, which points to a probable sedimentary contribution (Laurent et al., 2011). In
425 order to better understand the variations presented by the Hf and O isotopes, we have
426 constructed a concentration-weighted ternary mixing model showing the possible
427 results of crustal assimilation by mantle-derived melts (Fig. 6a). The model incorporates
428 proportions of mixing with end members of variable concentrations, and thus results in
429 arcuate-bounded regions in a ternary mixing model diagram. End-members we consider
430 are (1) the mantle (less depleted mantle at c. 2.2 Ga; see implications below), (2) the
431 average composition of a TTG-melt derived from a high-T-altered oceanic crust (T_{DM} = ~
432 2.5 Ga), and (3) three sediments of different ages. Parameters used are listed in Table 2.
433 The ratios between the 2.2 Ga mantle and the crustal components (Hf_M/Hf_S) are 0.067
434 given the Hf concentration of the mantle (0.3 ppm – Stille et al., 1986) and the average Hf
435 concentration of Palaeoproterozioc sediments (~ 4.5 ppm); and 0.075 given the same
436 mantle composition and the average Hf concentration of Archaean sediments (~4 ppm)
437 (Vervoort et al., 1999). For mixing between the sediments and TTG-melt the Hf_S/Hf_{TTG}
438 ratio is 0.9, and between the mantle and TTG-melt the ratio is 0.06 (Hf_M/Hf_{TTG}). Each
439 proposed sediment end-member is modelled separately in combination with the other
440 two end-members (i.e. TTG-melt and mantle), yielding three trianguloid areas (Fig. 6 b,
441 c, d).

442 The modelling particularly addresses the composition of sanukitoid magmas
443 given their well-known complexity outlined above. Sediment composition is a strikingly
444 sensitive petrogenetic control because of its higher Hf concentration and elevated $\delta^{18}O$
445 isotopic signature. Successful models (passing close to sanukitoid compositions) were
446 obtained from both Palaeoproterozoic sediment end-members (Fig. 6b triangles 1,2 and
447 6c triangles 5,6), but the Archean model was implausible (Fig. 6d). Of the
448 Palaeoproterozoic possibilities, the 'self-feeding arc' (sediment 1), in which sediments

derive from the arc itself, represents the best explanation for the sanukitoid magmas, because sediment 2 would require a mixture with insufficient mantle/too much TTG input, inconsistent with bulk geochemical characteristics.

Table 2: Possible reservoirs and estimations for $\varepsilon Hf_{(t)}$ values, O isotope composition and Hf concentration used in the ternary mixing diagrams. The three mixing ternary areas differ only by the sediment source (i.e. Archaean or Palaeoproterozoic).

Reservoir	$\varepsilon Hf_{(t)}$	Reasoning	$\delta^{18}O$ (‰)	Reasoning	Hf (ppm)	Reference
Depleted mantle at 2.5 Ga	8	Intercept with the DM line (red star)	5.5	Equilibrium with mantle melts during extraction Valley (2003)	0.157	Workman and Hart (2005)
2.2 Ga mantle	3	Intercept between crustal array and mantle evolution line (purple star)	5.5	Equilibrium with mantle melts during extraction Valley (2003)	0.3	Stille et al. (1986)
TTG-melt	5	Average of Hf isotopes analysed in this study for LDS	4.5	High-T altered mafic source mix with unaltered mafic source	5	Seixas et al. (2012) – highest concentration
Sediment 1 (Palaeoproterozoic)	-2	Hypothetical sediment derived from the own arc (average $\varepsilon Hf_{(t)}$ = 0) with little evolved signature	12	Shieh and Schwarcz (1978)	4.5	Vervoort et al. (1999) – average of juvenile sediments
Sediment 2 (Palaeoproterozoic)	-12	Lowest signature of c. 2.1 Ga detrital zircon grains (high evolved signature)	12	Shieh and Schwarcz (1978)	4.5	Ditto
Sediment 3 (Archaean)	-20	Hypothetical sediment derived from evolved crust (CHUR at 3 Ga)	12	Shieh and Schwarcz (1978)	4	Vervoort et al. (1999) – average of Archaean sediments

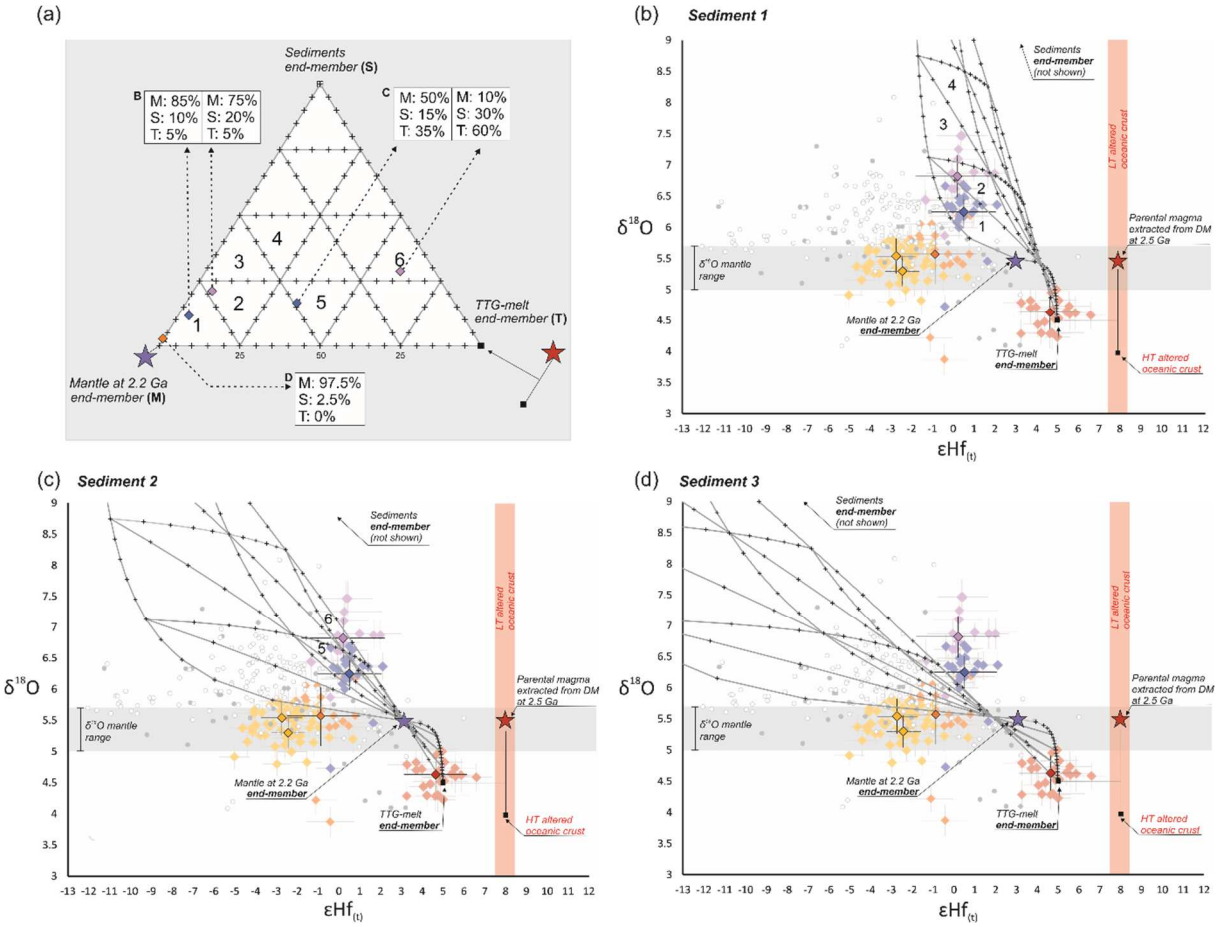

Figure 6: Zircon-based ternary mixing models and εHf versus $\delta^{18}O$ diagrams. Dark grey lines show the mixing between mantle-derived magmas, TTG-melts and sediment end-members (see methodology for constants and estimations applied). Each black cross in these curves represents a 5% interval between the end-member compositions. (a) Hypothetical triangle for elucidation of the modelling. It represents ternary mixing from which the reservoirs are equally distant and have the same Hf concentrations. Average of the zircon grains analysed for each of the suites of rocks are plotted in this diagram to show how the estimation of the constituents were determined, respectively for models in (b), (c) and (d). Sub-triangular domains presented in (a) are also located in diagrams (b) and (c) for comparison. (b) Modelling based on sediments 1 from table 2. (c) Modelling based on sediments 2 from table 2. (d) Modelling based on sediments 3 from table 2.

Although based on approximations of global sedimentary rocks, the modelling is consistent with accepted models of TTG generation, and provides convincing evidence for sediment contamination of mantle melts in sanukitoid petrogenesis. Extending the model to a plausible tectonic explanation, we have distinguished 3 chronological stages (Fig. 7).

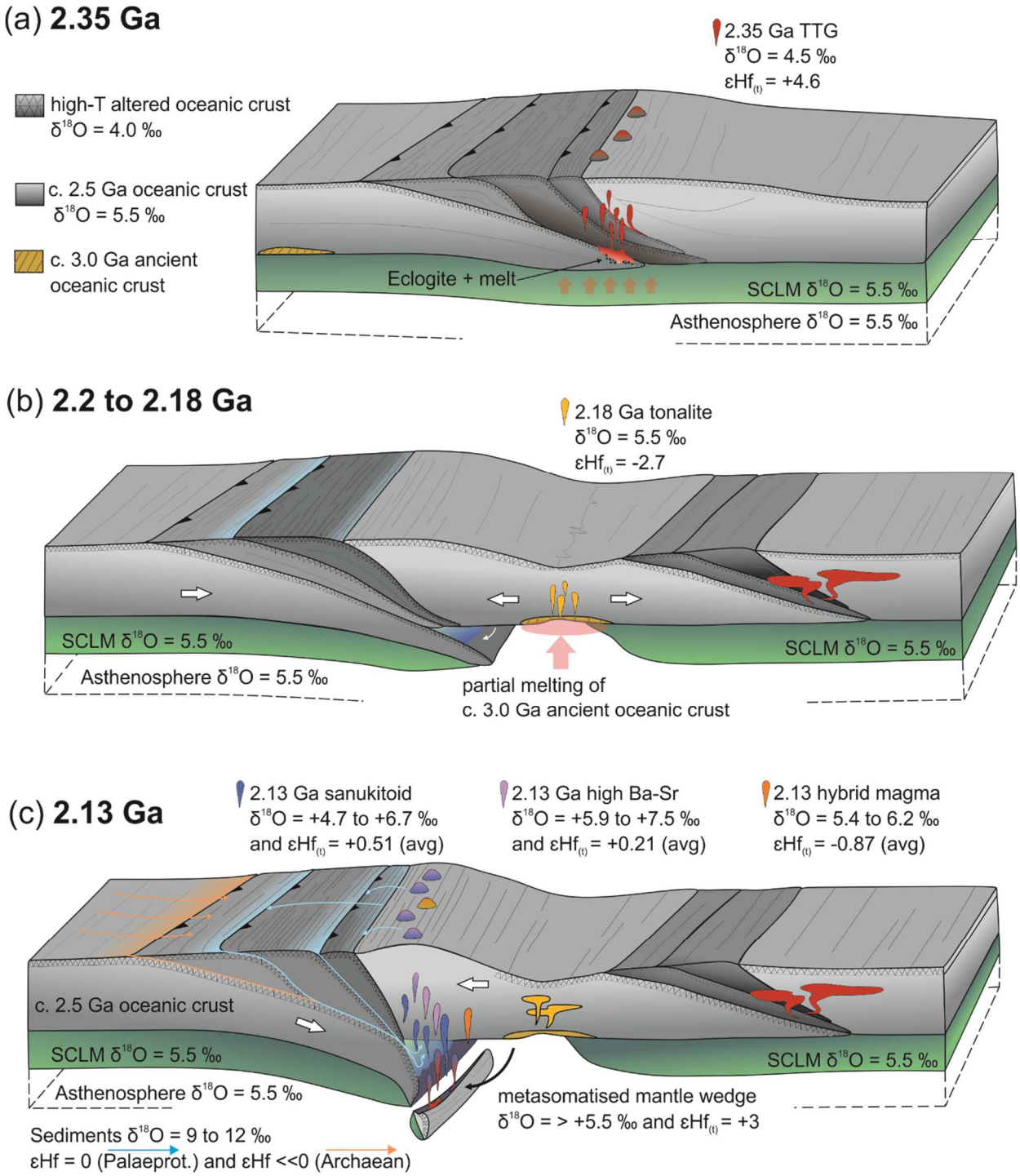

Figure 7: Tectonic model conceived for steepening of subducted oceanic slab due to TTG-magma generation and eclogite residue (not to scale). (a) Melting of a mixture of altered and pristine oceanic crust generates the TTG magmas and eclogitization of the under plate. (b) Steepening of the plate and initiation of the mantle wedge at c. 2.2 Ga. Consequently, a 'back-arc' type basin triggers re-melting of older Archaean mafic crust in the lower crust at c. 2.18 Ga. (c) Sediments driven from the subducted plate metasomatise the mantle and mix with small portions of the TTG-like magmas to generate the sanukitoids and high Ba-Sr magmas by fractional crystallisation at 2.13 Ga. Hybrid granitoid (and to a certain extent the high Ba-Sr magmas) generation involved participation of small amounts of Archaean sediments.

Stage 1: Palaeoproterozoic-derived TTG

In the model, the tonalites are derived from a high-T-altered mafic crust with $\varepsilon Hf_{(t)}$ composition of +8 and $\delta^{18}O_{WR}$ of 4 ‰ (Eiler, 2001). This source is consistent with a tholeiitic mantle magma extracted at 2.5 Ga, altered on the sea-floor by high-temperature waters and shortly after melted to generate the existing 2.35 Ga tonalites. There is also the possibility of mixing melts from different mafic sources with different degrees of hydrothermal alteration. By mass balance, a mixture of 60 % of altered mafic crust ($\delta^{18}O_{WR}$ = 4 ‰) and 40 % of unaltered mafic crust ($\delta^{18}O_{WR}$ = 5.5 ‰) would generate zircon grains in the tonalite with $\delta^{18}O$ of 4.6 ‰.

Stage 2: Archaean-derived tonalites

Hf isotopes of the c. 2.180 Ga suite yielded the oldest model ages for the plutonic rocks of this study (c. 3.0 Ga). However, mantle-derived $\delta^{18}O$ values and less evolved geochemical features (low SiO_2, K, Ba, and Sr) suggest minor supracrustal contribution. Based on the superposition of negative $\varepsilon Nd_{(t)}$ values of sample 16-MSC-1D and the Nd evolution line of one of the amphibolite rafts within the main tonalite (Seixas et al., 2012), Moreira et al. (2018) suggested that crustal melting occurred during the formation of the tonalite at 2.180 Ga, as assimilation of an Archaean mafic crust could be linked to the presence of amphibolite xenoliths. Alternatively, the rafts could represent portions of a mafic source not completed consumed by the derived tonalitic melt. One way to identify how much of this Archaean mafic crust was involved is modelling the $\delta^{18}O$ and Hf composition from the depleted mantle towards the $^{176}Hf/^{177}Hf$ composition of the zircons from the tonalite. The ternary mixing model (Fig. 6) shows that sediments or old crust did not contribute significantly to the tonalite composition, which seems to have been dominated by a modelled magma with $\varepsilon Hf \sim +6.5$ units and $\delta^{18}O \sim 5$ ‰.

Therefore, melting of an unaltered Archaean mafic source better explains the isotopic signatures and implies a quiescent residence time of roughly 800 Myr. One tectonic scenario for the genesis of such tonalites involves lithosphere thinning and asthenosphere upwelling during roll-back of a subducting plate, resembling a back-arc basin (Fig. 7b). This would provide sufficient heat for crustal melting and could have occurred shortly after the mantle-wedge initiation suggested to have occurred at 2.2 Ga (see below).

Stage 3: Sanukitoids, high Ba-Sr magmas and hybrid granitoids

Sanukitoids and high Ba-Sr magmas show evidence for mantle interaction with a TTG-like melt and/or sediments (e.g. Martin et al., 2009; Laurent et al., 2011, Fowler et al., 2008). The model presented here uses a mantle component with εHf = +3 and $\delta^{18}O$ = 5.5‰. This is justified by the better fit in the crustal evolution array lines in εHf versus time space (Fig. 4 and 8) and the overlap with a less-depleted mantle evolution line (based on Hf isotopes of deep-mantle plumes, Stille et al., 1986). Following the mantle wedge hypothesis for sanukitoid derivation, this is consistent with proto-subduction starting at c. 2.2 Ga, whereby the incremental density of eclogite residue at the base of the crust reached the 'tipping point', and this dense material foundered into the mantle (e.g. Bédard et al., 2018). Then, seventy Myr later a mantle wedge had formed from which the sanukitoid magmas were derived at 2.13 Ga. As soon as weathering and erosion of the developing arc started, the derived ^{18}O-enriched sediments were promptly recycled back in to the mantle, retaining a relatively juvenile Hf signature. Therefore, the εHf signature of the sediments used for the model is set at -2 (lowest possible value – taking into account uncertainties – obtained in igneous zircon for the sanukitoid/high Ba-Sr magmas). This process can be described as self-feeding of the arc, indicated by

535 increasing $\delta^{18}O$ values from 4.7 ‰ to 7.5 ‰. Ternary modelling implies the precursor
536 magma was extracted from a portion of the mantle wedge modified by c. 10 to 20% of
537 subducted sediments (Fig. 6b and Fig. 7). Most of the constituents are mantle-derived
538 (85 and 75% for sanukitoid and high Ba-Sr granitoids respectively) with only 5 to 10 %
539 derived from TTG-like melts. Alternatively, using a contemporary mantle at 2.13 Ga with
540 chondritic signature, the modelling yields c. 5% lower mantle contribution to the
541 magmas, but maintain the secondary role of the sediments and TTG components (see
542 supplementary material). The proportion of sediments calculated to be involved in the
543 sanukitoid composition with realistic model ages does not change for the two different
544 mantles used in the model (i.e. 2.2 or 2.13 Ga mantle), which has implications for the
545 composition of the sedimentary sources undergoing exhumation and erosion at low
546 temperatures.

547 A special case is shown by the zircons from trondhjemites and granodiorites of
548 the hybrid granitoid pluton, originally incorporated in the high Ba-Sr Suite by Moreira et
549 al. (2018). The pluton has lower Mg# and Ba + Sr + Fe concentration compared to the
550 other granitoids of the high Ba-Sr Suite, and straddles the hybrid granites field of
551 Laurent et al. (2014) (Fig. 3d). The dispersion towards more negative εHf values in the
552 ternary modelling and overall older T_{DM} ages (for both Hf and Nd isotopes) suggest a
553 small contribution from older Archaean sediments. The overlap of the $\delta^{18}O$ versus εHf
554 space of the detrital Archaean zircons presented here supports this hypothesis (Fig. 4d).

555

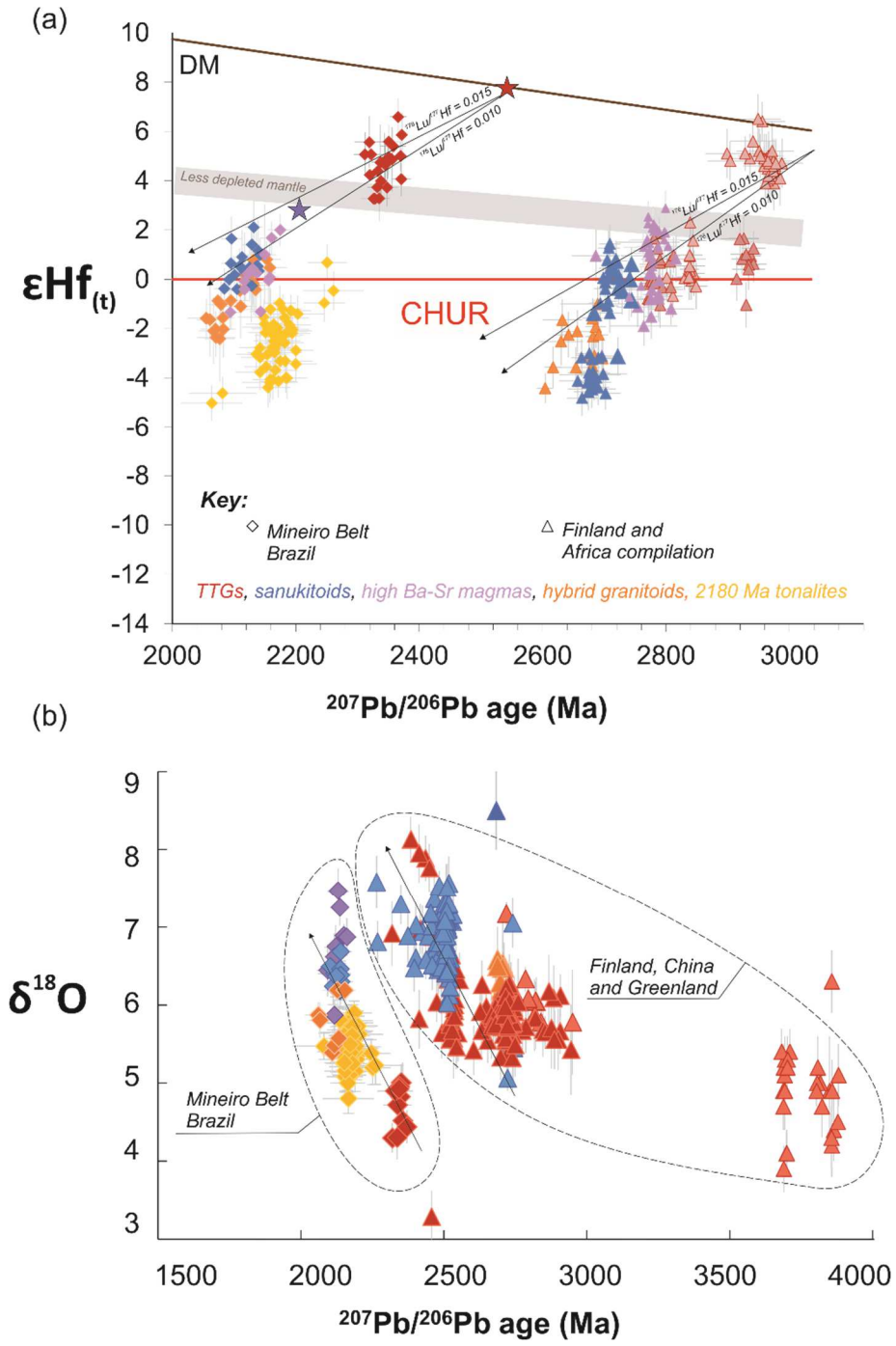

Figure 8: Comparison of (a) Hf and (b) oxygen isotopes of zircon grains from TTG-sanukitoid and comparable magmas worldwide (Zeh et al., 2009; 2013; Heilimo et al., 2011; 2013) and the Mineiro Belt. Black arrows in (a) represent plausible crustal reservoirs ($^{176}Lu/^{177}Hf$ >0) and point to similar evolution arrays regardless of the eon in which they occur. The colour codes match the following lithotypes: red for TTG, blue for sanukitoids, pink for high Ba-Sr magmas and orange for hybrid magmas. The Palaeoproterozoic zircon grains in diamond shapes represent analyses from the Mineiro Belt, and the triangles are from localities in Finland and Africa. They project similar crustal evolution arrays through time, regardless of their age. Oxygen isotope analyses from Archaean zircon grains from Finland, China and Greenland (Hiess et al., 2009; Mikkola et al., 2011; Heilimo et al., 2013; Jiang et al., 2016) are isotopically comparable to our rocks in the Palaeoproterozoic. Although the same trends are observed in younger orogenies, the resemblance cannot be associated to Archaean tectonics because the magmatism related is drastically different. The huge majority of magmas formed in the Phanerozoic contrast greatly with the TTGs presented in this study because they belong to the BADR series (see Figure 1).

6 – The Global Transition to Plate Tectonics

TTG and/or sanukitoid magmas have now been recorded from the Palaeoarchaean to Neoarchaean in almost all cratons worldwide and in most cases with a clear evolutionary trend from TTG to sanukitoid (e.g. Laurent et al., 2014; Halla et al., 2017). The timespan over which this evolution occurred is generally considered to be in the Archaean (e.g. Nebel et al., 2018). TTG generation mostly involved melting of basaltic sources after their production in the upper mantle (Moyen and Laurent, 2018). It has been suggested that a system governed by stacking of oceanic slabs (Hastie et al., 2016), subsequently led to eclogitization and steepening of the downthrust/proto-subduction angle to open the mantle wedge (Bédard et al., 2018). Subsequent interaction with volatiles, sediments and TTG-like melts from the downgoing slab(s) enriched the mantle wedge and generated sanukitoid magmas in the igneous record for the first time at c. 3.0 Ga (Laurent et al., 2011; 2014). The system marks the growth of the depleted mantle and the continental crust and must, therefore, be connected with the generation of the subcontinental lithospheric mantle (SCLM) (Fowler & Rollinson, 2012). When the upper mantle became mostly depleted, this system slowed to a halt (Moyen and Laurent, 2018), which coincides with the proposed magmatic lull (Spencer et al., 2018).

The TTG-sanukitoid transition, therefore, marks not only a geochemical evolution, but also a tectonic context of continent-driven imbrication of oceanic slabs (Bédard, 2018). This secular evolution is not unequivocally a mark of a modern-style of subduction-driven plate tectonics for two reasons: 1) the higher mantle temperature (c. 250 °C above present day, Condie et al., 2016) and the relatively weaker and more buoyant oceanic crust do not allow the generation of tensional stress after slab pull transmission; consequently, 2) downwelling forces are not efficient in dragging down

595 cold slabs to higher pressures and generating the low dT/dP rocks, which comprise a
596 hallmark of the subduction-driven plate world (Stern, 2018). The transition, rather,
597 represents a gestational period of a repeated failure of the start of subduction in plate
598 tectonics (Cawood et al., 2018; Nebel et al., 2018), consumption of the undepleted
599 mantle, generation of the SCLM and continental crust growth (Moyen and Laurent, 2018;
600 Bédard, 2018; Dhuime et al., 2018).

601 The new data presented here from the Mineiro belt demonstrate that similarities
602 between Archaean and Palaeoproterozoic TTG-sanukitoid suites are not only recorded
603 by the bulk geochemistry (Moreira et al, 2018), but also by the isotopic systems, which
604 show closely similar evolutionary patterns. In Figure 8, for example, Hf isotope data
605 compiled from Archaean TTG-sanukitoid sequences (and associated hybrid magmas) are
606 undeniably analogous to the linear evolution presented by the samples of this study:
607 TTGs were derived from short-lived basaltic sources; they evolved towards
608 subchondritic values and were replaced by sanukitoid magmatism during a timeframe of
609 roughly 200 Myr. This pattern happens, diachronously, in almost all cratons worldwide
610 and is also observed in the Sm-Nd isotopic system, interpreted as incremental
611 reworking and recycling of the crust (Laurent et al., 2014). Supramantle $\delta^{18}O$ values are
612 similar to the range of other sanukitoid magmas worldwide (Fig. 5), suggesting a similar
613 influence of sediments within the nascent mantle wedge. At the other extreme,
614 comparable low $\delta^{18}O$ values (as low as +4.0‰) have been ascribed to high-temperature
615 altered gabbroic sources of the TTG rocks dating back to 3.8 Ga (Fig. 5). In short, there is
616 no fundamental difference in petrogenetic process in the TTG-sanukitoid transition from
617 Neoarchaean to Palaeoproterozoic examples.

618 It is also evident that deep penetration of oceanic lithosphere into the mantle is
619 required to generate the mantle wedge. Thus, sanukitoids can be rationalised by slab
620 break-off after attempted subduction of buoyant continental lithosphere (Halla et al.,
621 2009), which implies a collisional setting controlled by lateral drift of rigid plates and
622 presence of a mantle wedge. Importantly, it also clearly demonstrates that mantle wedge
623 interaction does not prove modern-style subduction. However, at c. 2.0 Ga, following the
624 assemblage of the Columbia/Nuna supercontinent, cold and steep subduction had
625 established a new plate tectonic style (e.g. Brown and Johnson, 2018). This may have
626 been irreversibly triggered by the supercontinent cycle after insulation and
627 reorganization of the mantle (Spencer et al., 2018). Therefore, we propose that this final
628 TTG-sanukitoid transition is the last gasp of an ante-plate tectonics regime, marked by
629 multiple, sequential, stalled attempts to initiate the modern-style of subduction on
630 Earth.

631 ***7 – Conclusions***

632 The occurrence of a narrow evolution window from TTG to sanukitoid and
633 related magmas in the Mineiro Belt during the 'global magmatic lull' provides
634 indisputable evidence for crustal growth, reworking and recycling during the early
635 Palaeoproterozoic.

636 This TTG-sanukitoid transition involves proto-subduction-driven plate tectonics,
637 here termed as ante-plate tectonics, and it is petrogenetically similar to the Neoarchaean
638 evolution of granitoid rocks reported worldwide.

639 The 2.35 Ga TTG derives from a short-lived high-temperature hydrothermally
640 altered metabasaltic source; the interaction of similar TTG-like melts, within the mantle

641 wedge, and subducted sediments marks the generation of sanukitoids some 200 Myr
642 later.

643 The opening of the mantle wedge began at c. 2.2 Ga, during proto-subduction
644 initiation. Seventy million years elapsed between the opening of the mantle wedge and
645 production of sediment-contaminated magmas, in the form of sanukitoid, high Ba-Sr and
646 hybrid granitoid suites at c. 2.13 Ga.

647 The opening of the mantle wedge also triggered the melting of Archaean basaltic
648 source and generation of 2.18 – 2.2 Ga tonalitic magmas.

649 This latest TTG-sanukitoid transition represents the last vestige of an ante-plate
650 tectonics regime initiated during the Palaeoproterozoic magmatic lull. After this tipping
651 point, the Earth was inescapably locked into the modern plate tectonic regime.

652 **Acknowledgments**

653 Hugo Moreira acknowledges CNPq (National Council for Scientific and Technological
654 Development) grant (234610/2014-0), Jean-François Moyen for his critical and valuable input
655 about the overall evolution of magmatic and subduction systems, and Randall Parrish for
656 detailed review of this manuscript, enlightening discussions and encouragement. We thank Tony
657 Kemp and an anonymous reviewer for insightful comments on a previous version of this
658 manuscript. We are extremely grateful to the NERC facilities grant IMF615/1016, the EIMF
659 (Edinburgh Ion Microprobe Facility), and especially to John Craven for his dedication and
660 analytical support during the stable oxygen isotope analyses. Geoff Long is thanked for
661 preparing resin mounts of exceptional quality.
662

663 **References**

664 Ávila, C.A., Teixeira, W., Bongiolo, E.M., Dussin, I.A. and Vieira, T.A.T., 2014. Rhyacian evolution of
665 subvolcanic and metasedimentary rocks of the southern segment of the Mineiro belt, São
666 Francisco Craton, Brazil. Precambrian Research, 243, pp.221-251.

667 Beall, A.P., Moresi, L. and Cooper, C.M., 2018. Formation of cratonic lithosphere during the
668 initiation of plate tectonics. Geology, 46(6), pp.487-490.

669 Bédard, J.H., 2018. Stagnant lids and mantle overturns: implications for Archaean tectonics,
670 magmagenesis, crustal growth, mantle evolution, and the start of plate tectonics. Geoscience
671 Frontiers 9, 19-49.

672 Brown, M. and Johnson, T., 2018. Secular change in metamorphism and the onset of global plate
673 tectonics. American Mineralogist, 103(2), pp.181-196.

674 Cawood, P.A., Hawkesworth, C.J. and Dhuime, B., 2012. Detrital zircon record and tectonic
675 setting. Geology, 40(10), pp.875-878.

676 Cawood, P.A., Hawkesworth, C.J., Pisarevsky, S.A., Dhuime, B., Capitanio, F.A. and Nebel, O., 2018.
677 Geological archive of the onset of plate tectonics. Philosophical Transactions of the Royal Society
678 A: Mathematical, Physical and Engineering Sciences, 376(2132), p.20170405.

679 Condie, K.C., Aster, R.C. and Van Hunen, J., 2016. A great thermal divergence in the mantle
680 beginning 2.5 Ga: Geochemical constraints from greenstone basalts and komatiites. Geoscience
681 Frontiers, 7(4), pp.543-553.

682 Dhuime, B., Hawkesworth, C.J., Delavault, H. and Cawood, P.A., 2018. Rates of generation and
683 destruction of the continental crust: implications for continental growth. Philosophical
684 Transactions of the Royal Society A: Mathematical, Physical and Engineering Sciences,
685 376(2132), p.20170403.

686 Eiler, J.M., 2001. Oxygen isotope variations of basaltic lavas and upper mantle rocks: Reviews in
687 Mineralogy and Geochemistry, v. 43, p. 319–364, doi: 10.2138 /gsrmg .43 .1 .319.

688 Foley, S.F., Buhre, S. and Jacob, D.E., 2003. Evolution of the Archaean crust by delamination and
689 shallow subduction. Nature, 421(6920), p.249.

690 Fowler, M.B., Kocks, H., Darbyshire, D.P.F. and Greenwood, P.B., 2008. Petrogenesis of high Ba–Sr
691 plutons from the northern highlands Terrane of the British Caledonian Province. Lithos, 105(1-
692 2), pp.129-148.

693 Fowler, M., Rollinson, H., 2012. Phanerozoic sanukitoids from Caledonian Scotland: implications
694 for Archean subduction. Geology, 40(12), pp.1079-1082.

695 Gregory, R.T. and Taylor Jr, H.P., 1981. An oxygen isotope profile in a section of Cretaceous
696 oceanic crust, Samail Ophiolite, Oman: Evidence for δ18O buffering of the oceans by deep (> 5
697 km) seawater-hydrothermal circulation at mid-ocean ridges. Journal of Geophysical Research:
698 Solid Earth, 86(B4), pp.2737-2755.

699 Halla, J., van Hunen, J., Heilimo, E. and Hölttä, P., 2009. Geochemical and numerical constraints on
700 Neoarchean plate tectonics. Precambrian Research, 174(1-2), pp.155-162.

701 Halla, J., Whitehouse, M.J., Ahmad, T. and Bagai, Z., 2017. Archaean granitoids: an overview and
702 significance from a tectonic perspective. Geological Society, London, Special Publications,
703 449(1), pp.1-18.

704 Hastie, A.R., Fitton, J.G., Bromiley, G.D., Butler, I.B. and Odling, N.W., 2016. The origin of Earth's
705 first continents and the onset of plate tectonics. Geology, 44(10), pp.855-858.

706 Hawkesworth, C.J. and Kemp, A.I.S., 2006. Using hafnium and oxygen isotopes in zircons to
707 unravel the record of crustal evolution. Chemical Geology, 226(3-4), pp.144-162.

708 Heilbron, M., Cordani, U.G., Alkmim, F.F. and Reis, H.L., 2017. Tectonic genealogy of a miniature
709 continent. In São Francisco Craton, Eastern Brazil (pp. 321-331). Springer, Cham.

710 Heilimo, E., Halla, J., Andersen, T. and Huhma, H., 2013. Neoarchean crustal recycling and mantle
711 metasomatism: Hf–Nd–Pb–O isotope evidence from sanukitoids of the Fennoscandian shield.
712 Precambrian Research, 228, pp.250-266.

713 Heilimo, E., Halla, J. and Hölttä, P., 2010. Discrimination and origin of the sanukitoid series:
714 geochemical constraints from the Neoarchean western Karelian Province (Finland). Lithos,
715 115(1-4), pp.27-39.

716 Heilimo, E., Halla, J. and Huhma, H., 2011. Single-grain zircon U–Pb age constraints of the
717 western and eastern sanukitoid zones in the Finnish part of the Karelian Province. Lithos, 121(1-
718 4), pp.87-99.

719 Hiess, J., Bennett, V.C., Nutman, A.P. and Williams, I.S., 2009. In situ U–Pb, O and Hf isotopic
720 compositions of zircon and olivine from Eoarchaean rocks, West Greenland: new insights to
721 making old crust. Geochimica et Cosmochimica Acta, 73(15), pp.4489-4516.

722 Hopkinson, T.N., Harris, N.B., Warren, C.J., Spencer, C.J., Roberts, N.M., Horstwood, M.S. and
723 Parrish, R.R., 2017. The identification and significance of pure sediment-derived granites. Earth
724 and Planetary Science Letters, 467, pp.57-63.

725 Jiang, N., Guo, J., Fan, W., Hu, J., Zong, K. and Zhang, S., 2016. Archean TTGs and sanukitoids from
726 the Jiaobei terrain, North China craton: Insights into crustal growth and mantle metasomatism.
727 Precambrian Research, 281, pp.656-672.

728 Kemp, A.I.S., Hawkesworth, C.J., Paterson, B.A. and Kinny, P.D., 2006. Episodic growth of the
729 Gondwana supercontinent from hafnium and oxygen isotopes in zircon. Nature, 439(7076),
730 pp.580-583.

731 Laurent, O., Björnsen, J., Wotzlaw, J.F., Bretscher, S., Silva, M.P., Moyen, J.F., Ulmer, P. and
732 Bachmann, O., 2020. Earth's earliest granitoids are crystal-rich magma reservoirs tapped by
733 silicic eruptions. Nature Geoscience, pp.1-7.

734 Laurent, O., Martin, H., Doucelance, R., Moyen, J.F. and Paquette, J.L., 2011. Geochemistry and
735 petrogenesis of high-K "sanukitoids" from the Bulai pluton, Central Limpopo Belt, South Africa:
736 Implications for geodynamic changes at the Archaean–Proterozoic boundary. Lithos, 123(1-4),
737 pp.73-91.

738 Laurent, O., Martin, H., Moyen, J.F. and Doucelance, R., 2014. The diversity and evolution of late-
739 Archean granitoids: Evidence for the onset of "modern-style" plate tectonics between 3.0 and 2.5
740 Ga. Lithos, 205, pp.208-235.

741 Martin, H., Moyen, J.F. and Rapp, R., 2009. The sanukitoid series: magmatism at the Archaean–
742 Proterozoic transition. Earth and Environmental Science Transactions of the Royal Society of
743 Edinburgh, 100(1-2), pp.15-33.

744 Martínez Dopico, C.I., Lana, C., Moreira, H.S., Cassino, L.F. and Alkmim, F.F., 2017. U–Pb ages and
745 Hf-isotope data of detrital zircons from the late Neoarchean-Paleoproterozoic Minas Basin, SE
746 Brazil. Precambrian Research, 291, pp.143-161.

747 Mikkola, P., Huhma, H., Heilimo, E. and Whitehouse, M., 2011. Archean crustal evolution of the
748 Suomussalmi district as part of the Kianta Complex, Karelia: constraints from geochemistry and
749 isotopes of granitoids. Lithos, 125(1-2), pp.287-307.

750 Moreira, H., Seixas, L., Storey, C., Fowler, M., Lasalle, S., Stevenson, R. and Lana, C., 2018.
751 Evolution of siderian juvenile crust to rhyacian high Ba-Sr magmatism in the Mineiro Belt,
752 southern São Francisco Craton. Geoscience Frontiers, 9(4), pp.977-995.

753 Moyen, J.F. and Martin, H., 2012. Forty years of TTG research. Lithos, 148, pp.312-336.

754 Moyen, J.F. and Laurent, O., 2018. Archaean tectonic systems: a view from igneous rocks. Lithos,
755 302, pp.99-125.

756 Nebel, O., Capitanio, F.A., Moyen, J.F., Weinberg, R.F., Clos, F., Nebel-Jacobsen, Y.J. and Cawood,
757 P.A., 2018. When crust comes of age: on the chemical evolution of Archaean, felsic continental
758 crust by crustal drip tectonics. Philosophical Transactions of the Royal Society A: Mathematical,
759 Physical and Engineering Sciences, 376(2132), p.20180103.

760 Payne, J.L., McInerney, D.J., Barovich, K.M., Kirkland, C.L., Pearson, N.J. and Hand, M., 2016.
761 Strengths and limitations of zircon Lu-Hf and O isotopes in modelling crustal growth. Lithos,
762 248, pp.175-192.

763 Seixas, L.A.R., Bardintzeff, J.M., Stevenson, R. and Bonin, B., 2013. Petrology of the high-Mg
764 tonalites and dioritic enclaves of the ca. 2130 Ma Alto Maranhão suite: Evidence for a major
765 juvenile crustal addition event during the Rhyacian orogenesis, Mineiro Belt, southeast Brazil.
766 Precambrian Research, 238, pp.18-41.

767 Seixas, L.A.R., David, J. and Stevenson, R., 2012. Geochemistry, Nd isotopes and U–Pb
768 geochronology of a 2350 Ma TTG suite, Minas Gerais, Brazil: implications for the crustal
769 evolution of the southern São Francisco craton. Precambrian Research, 196, pp.61-80.

770 Shieh, Y.N. and Schwarcz, H.P., 1978. The oxygen isotope composition of the surface crystalline
771 rocks of the Canadian Shield. Canadian Journal of Earth Sciences, 15(11), pp.1773-1782.

772 Shirey, S.B., Hanson, G.N., 1984. Mantle derived Archaean monzodiorites and trachyandesites.
773 Nature. 310, 222–224.

774 Smithies, R.H., 2000. The Archaean tonalite–trondhjemite–granodiorite (TTG) series is not an
775 analogue of Cenozoic adakite. Earth and Planetary Science Letters, 182(1), pp.115-125.

776 Spencer, C.J., Murphy, J.B., Kirkland, C.L., Liu, Y. and Mitchell, R.N., 2018. A Palaeoproterozoic
777 tectono-magmatic lull as a potential trigger for the supercontinent cycle. Nature Geoscience, p.1.

778 Stern, R.J., 2018. The evolution of plate tectonics. Philosophical Transactions of the Royal Society
779 A: Mathematical, Physical and Engineering Sciences, 376(2132), p.20170406.

780 Stille, P., Unruh, D.M. and Tatsumoto, M., 1986. Pb, Sr, Nd, and Hf isotopic constraints on the
781 origin of Hawaiian basalts and evidence for a unique mantle source. Geochimica et
782 Cosmochimica Acta, 50(10), pp.2303-2319.

783 Teixeira, W., Ávila, C.A., Dussin, I.A., Neto, A.C., Bongiolo, E.M., Santos, J.O. and Barbosa, N.S., 2015.
784 A juvenile accretion episode (2.35–2.32 Ga) in the Mineiro belt and its role to the Minas
785 accretionary orogeny: Zircon U–Pb–Hf and geochemical evidences. Precambrian Research, 256,
786 pp.148-169.

787 Valley, J.W., 2003. Oxygen isotopes in zircon. Reviews in mineralogy and geochemistry, 53(1),
788 pp.343-385.

789 Vervoort, J.D., Patchett, P.J., Blichert-Toft, J. and Albarède, F., 1999. Relationships between Lu–Hf
790 and Sm–Nd isotopic systems in the global sedimentary system. Earth and Planetary Science
791 Letters, 168(1), pp.79-99.

792 Workman, R.K. and Hart, S.R., 2005. Major and trace element composition of the depleted MORB
793 mantle (DMM). Earth and Planetary Science Letters, 231(1-2), pp.53-72.

794 Zeh, A., Gerdes, A. and Barton Jr, J.M., 2009. Archean accretion and crustal evolution of the
795 Kalahari Craton—the zircon age and Hf isotope record of granitic rocks from
796 Barberton/Swaziland to the Francistown Arc. Journal of Petrology, 50(5), pp.933-966.

797 Zeh, A., Jaguin, J., Poujol, M., Boulvais, P., Block, S. and Paquette, J.L., 2013. Juvenile crust
798 formation in the northeastern Kaapvaal Craton at 2.97 Ga—Implications for Archean terrane
799 accretion, and the source of the Pietersburg gold. Precambrian Research, 233, pp.20-43.

800 Zhao, Z.F., Zheng, Y.F., 2003. Calculation of oxygen isotope fractionation in magmatic rocks.
801 Chemical Geology, 193(1-2), pp.59-80.